JMEPEG (2016) 25:3238–3244
DOI: 10.1007/s11665-016-2096-2

1059-9495/$19.00

Stress Engineering of Multi-pass Welds of Structural Steel to Enhance Structural Integrity

Supriyo Ganguly, Jibrin Sule, and Mustapha Y. Yakubu

(Submitted November 1, 2015; in revised form February 26, 2016; published online May 26, 2016)

In multi-pass welding, the weld metal and the associated heat-affected zone are subjected to repeated thermal cycling from successive deposition of filler metals. The thermal straining results into multi-mode deformation of the weld metal which causes a variably distributed residual stress field through the thickness and across the weld of a multi-pass weldment. In addition to this, the as-welded fusion zone microstructure shows dendritic formation of grains and segregation of alloying element. This may result in formation of micro-corrosion cells and the problem would aggravate in case of highly alloyed materials. Local mechanical tensioning is an effective way of elimination of the weld tensile residual stress. It has been shown that application of cold rolling is capable not only of removing the residual stress, but depending on its magnitude it may also form beneficial compressive stress state. Multi-pass structural steel welds used as structural alloy in general engineering and structural applications. Such alloys are subjected to severe in-service degradation mechanisms e.g., corrosion and stress corrosion cracking. Welds and the locked-in residual stress in the welded area often initiate the defect which finally results in failure. In the present study, a multi-pass structural steel weld metal was first subjected to post-weld cold rolling which was followed by controlled heating by a fiber laser. Cold straining resulted in redistribution of the internal stress through the thickness and controlled laser processing helps in reforming of the grain structure. However, even with controlled laser, processing the residual stress is reinstated. Therefore, a strategy has been adopted to roll the metal post-laser processing so as to obtain a complete stress-free and recrystallized microstructure.

Keywords Laser processing, mechanical properties, microstructure, multi-pass welds, residual stress, rolling, steel

1. Introduction

Steels (especially S275 steels) are a very popular low carbon steel grade suitable for numerous general engineering and structural applications. In these applications, it is essential to form strong joints that allow transfer of load between the different steel components. In most cases, welding is generally the most common method of joining. The welding method reduced the corrosion problems often associated with fasteners. This process (welding) create most robust joint to the application.

The most common and widely used welding processes are those which employ fusion. Fusion arc welding process relies on intense local heating at a joint where a certain amount of the parent metal is melted and fused with additional metal from the filler wire. Fusion arc welding is extensively used in a number of construction industries, offshore structures, and other structural applications. The main benefits of fusion welding, as joining processes, are creation of robust joint, flexibility in terms of setting up the equipment, and low fabrication costs. Disadvantage of this process is that the mechanical properties of the structural alloy are been alter as result of welding. This process also causes distortion and residual stresses in the welded structure.

The distribution of residual stress in the weld is generally tensile in the longitudinal (along-weld) direction close to the weld line, and further away from the weld center line, compressive longitudinal residual stresses exist balancing those in the weld zone (Ref 1). The presence of tensile residual stresses has been reported to accelerate stress corrosion cracking and fatigue crack growth rates (Ref 2-5), which are detrimental to the integrity and the service behavior of the welded joint.

A number of methods have been used to mitigate the effects of residual stress in welding. These include post-weld heat treatment (Ref 6), shot peening, modification of the structural configurations, and the implementation of thermal tensioning techniques (Ref 7, 8). It has also been reported that application of cold rolling is capable not only of removing the residual stress but depending on its magnitude it may also form beneficial compressive stress state (Ref 9-13).

In addition to a complex distribution of residual stress state, multi-pass welds also remelt the existing dendritic grain structure, resulting in aggression of segregation of alloying elements. Dendritic grain structure is weaker and segregation of

This article is an invited submission to JMEP selected from presentations at the Symposium "Joining Technologies," belonging to the Topic "Joining and Interfaces" at the European Congress and Exhibition on Advanced Materials and Processes (EUROMAT 2015), held September 20–24, 2015, in Warsaw, Poland, and has been expanded from the original presentation.

Supriyo Ganguly and **Jibrin Sule**, Cranfield - Welding Engineering and Laser Processing Centre, Cranfield University, MK43 0AL Bedford, UK, Northern Ireland; and **Mustapha Y. Yakubu**, National Engineering and Technical Company Limited (NETCO), Heritage Court 146B Ligali Ayorinde Street, Victoria Island, Lagos, Nigeria. Contact e-mail: s.ganguly@cranfield.ac.uk.

alloying elements would result in formation of corrosion microcells as well as reduction in overall corrosion resistance due to localized depletion of alloying elements. Modification of the material's microstructure by heat treatment can have a dramatic effect on hardness and fracture toughness in both the fusion region and the heat-affected zone (HAZ), which consequently affects fatigue properties greatly.

Our previous work (Ref 14) shows very minimal grains refinement and reinstated as-welded residual stress state profile when post-weld cold rolling followed by laser processing was applied to the sample. Following this observation, different methods were used which is the main objective of this investigation.

The aim of this research is to apply this novel method of cold rolling two times, before and after laser processing to modify the microstructures, mechanical properties, and residual stress state of multi-pass welds of structural steel.

2. Experiment

2.1 Material

In this study, the material used was S275JR structural steel plate (12 mm thick), and the filler wire used is Union MoNi (1.0 mm diameter). The chemical compositions (in weight percent) of the S275JR structural steel are 0.11 C, 0.23 Si, 1.08 Mn, 0.013 P, 0.02 Ni, 0.03 Al, 0.02 Cr, 0.03 Cu, 0.005 S, and others which include little quantity of Mo, Nb, Ti, and V. The filler wire used has the following chemical compositions (in weight percent): 0.12 C, 0.4-0.8 Si, 1.3-1.9 Mn, 0.015 P, 0.8-1.3 Ni, 0.25-0.65 Mo, Al, 0.15 Cr, 0.3 Cu, 0.018 S, and others. The shielding gas used was 92% Ar and 8% CO_2 at flow rate of 30 l min^{-1}. Figure 1 shows the welding set-up and the bevel was filled with four (4) welding passes.

2.2 Experimental Method

In this research the samples were processed in three stages after welding as given below. Metallography, mechanical properties, and residual stress measurement were carried out after each stage as shown in the flow chart in Fig. 2.

2.2.1 Welding. The welding was carried out using Tandem Gas Metal Arc Welding process. Welding parameters used are shown in Table 1.

The heat input was calculated using Eq 1.

$$\text{Heat input} = (\text{current x voltage x efficiency})/(\text{Travel speed}) \quad \text{(Eq 1)}$$

An efficiency factor of 80% was used (Ref 4).

Note that, the instantaneous current and voltage were recorded using a Scopecorder 750. The values were averaged for a certain period of stabilized welding, and these are used for computing the heat input.

2.2.2 Rolling Device. Post-weld cold rolling was carried out using the in-house rolling machine. This rolling device is capable of rolling with a constant force. The principle of operation of this machine was explained elsewhere (Ref 14). This roller was made from hardened BS 4659 BH13 tool steel. It has an effective width of 30 mm and the diameter of 100 mm. The rolling load of 150 kN with a constant travel speed of 700 mm min^{-1} was applied to welded sample.

2.2.3 Laser Processing. Laser processing was applied after post-weld cold rolling. An optical fiber of 300 μm diameter was used to transmit the laser beam to the laser head. Laser beam was collimated using a lens of 125 mm focal length. After collimating, focussing lens of 250 mm focal length was used to focus the beam. The focussing lens produce a spot size of 0.61 mm at the focal point as shown in Fig. 3. It worth mentioning here that the laser in this specific experiment was used to increase the temperature at a controlled rate. It was on this basis that the sample was heated up to 900 °C by controlling the laser power at constant beam diameter of 110 mm. Figure 3 shows the schematic diagram for design laser set-up. The laser head was positioned at 25° angle to avoid any back reflection that can damage the lens.

2.3 Experimental Measurement

In this experimental measurement, the weld thermal cycle, hardness scanning, and residual stress measurement were performed.

2.3.1 Determination of the Weld Thermal Cycles. Thermocouples were used to measure the thermal cycle of the weld metal with the aid of a Scopecorder 750 instrument. A hole was drilled through the plate thickness from the root side through the backing bar into which K-type thermocouples was placed. The thermocouples were placed at 1.0 mm below the weld surface (cap pass) and at 10.0 mm below the weld surface (root pass), respectively.

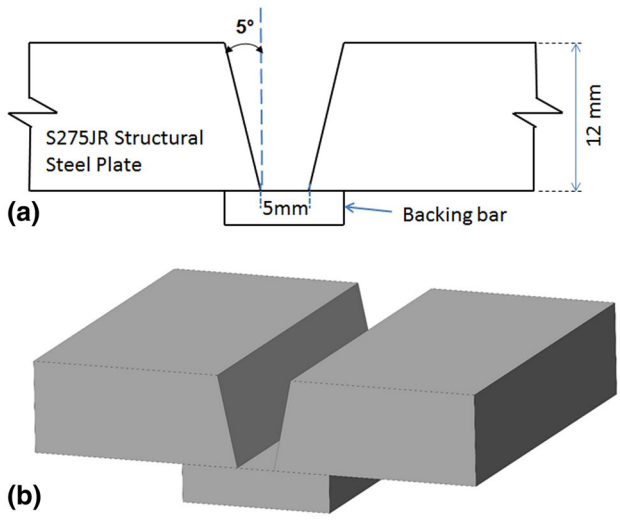

Fig. 1 S275JR structural steel plate welding set-up (a) side view (b) 3D view

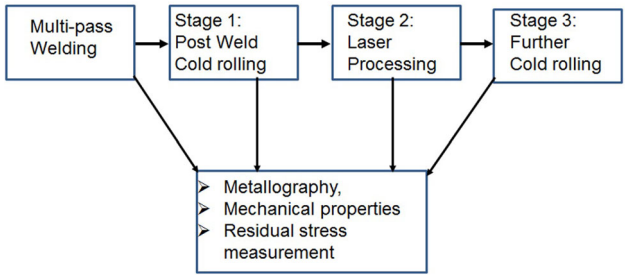

Fig. 2 Experimental flow chart

Table 1 Welding parameters on narrow groove welds of the S275JR structural steel plate

Passes	Travel speed, m/min	Lead			Trail			Heat input		
		Wfs, m/min	Av. current, A	Av. volts, v	Wfs, m/min	Av. current, A	Av. volts, v	Lead heat input, kJ/mm	Trail heat input, kJ/mm	Total heat input, kJ/mm
Root pass	0.9	11	190	20.3	11	160	25.5	0.21	0.22	0.43
Fill 1	0.9	12	191	21.5	12	185	21.7	0.22	0.21	0.43
Fill 2	0.9	13	209	22.2	13	192	21.7	0.25	0.22	0.47
Cap pass	0.7	11	215	21.5	11	208	21.4	0.32	0.30	0.62

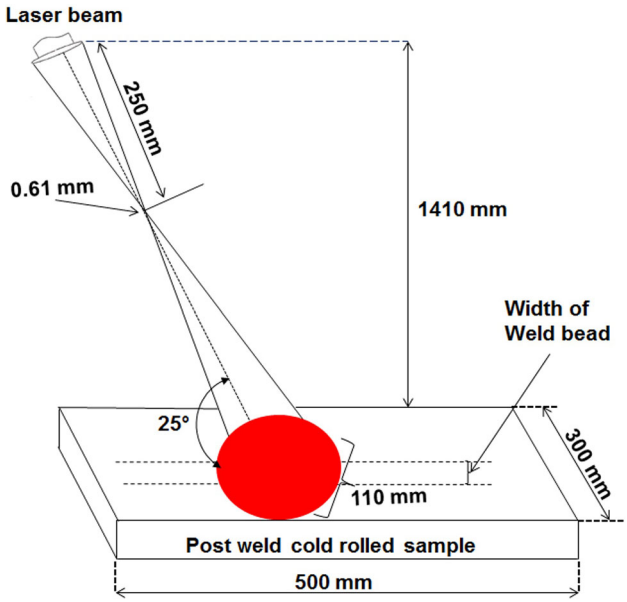

Fig. 3 Schematic diagram of laser processing set-up

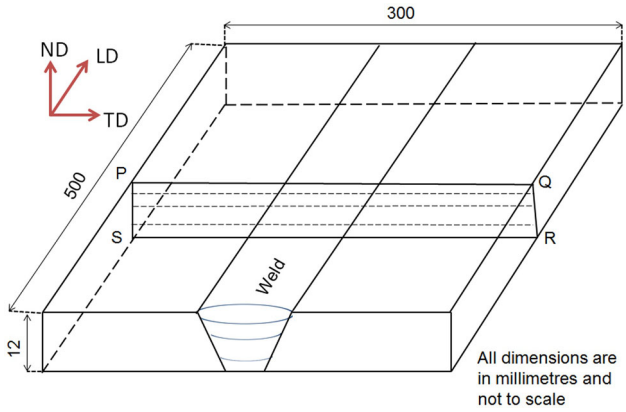

Fig. 4 Schematic diagram of the multi-pass welded plate showing lines of measurement

2.3.2 Hardness Measurement. Welded samples were prepared according to standard metallography procedures for microstructural observations and micro hardness tests. For microhardness testing, 0.5 kg load and 10 s dwell time were applied. Hardness scan was carried out across and along the weld metal at an interval of 1.0 mm within successive points.

2.3.3 Residual Stress Measurement. Due to neutron beam's unique deep penetration and three-dimensional mapping capability (Ref 15), neutron diffraction is widely used for stress measurements in a wide range of engineering structures. In this experiment, SALSA neutron diffractometer at the Institut Laue Langevin in France was used to measure the residual elastic strain (Ref 16). Residual stress state of the weld in the research was evaluated from the measurement of the elastic strain (Ref 17). The elastic strain measurements were made on the mid cross-sectional plane of a 500-mm sample (plane PQRS) as shown in Fig. 4. The mid-cross-sectional plane was chosen with the assumption that the stress state in the middle will reflect the stress generated from the steady-state welding process. The measurements were taken at 2.5, 6.5, and 10.5 mm below the plate surface on which the capping pass was laid. The longitudinal, transverse, and normal strains were measured. It was assumed that these directions measured, by symmetry, to be the principal stress directions. The coordinate axes LD, TD, and ND, as shown in Fig. 4, represent the longitudinal (parallel to the length of the weld), transverse (perpendicular to the length of the weld and parallel to the plate) and normal (perpendicular to the length of the weld and perpendicular to the plate), respectively.

The inter-planar spacing (d) of the {211} crystallographic plane was chosen for measurements of all the principal strain directions. The strain response of {211} family of crystallographic planes in the BCC lattice structure closely follows the macroscopic strain response over the measured gage volume (Ref 16). The measurements were made using a neutron incident beam of wavelengths, 1.6 Å, which gives a diffraction angle (2θ) of 84.5°. In order to achieve accuracy, it is important to perform a wall scan as reported by Wang, X. L. et'al (Ref 18). Therefore, in this work, the through-thickness scan was performed for accurate positioning of the gage volume within the plate. In order to maintain the through thickness resolution, the gage volume dimension was determined by using slits in front of the in-coming beam and collimating the diffracted beam. To achieve the desired spatial resolution, an incoming beam of 2×2 mm^2 was used for the longitudinal strain measurement while a 2-mm collimator was used for the diffracted beam. In these measurement conditions, the gage volume at the measuring position was set to be approximately $2 \times 2 \times 2$ mm^3. In the transverse and normal strain measurement, an incoming beam of 2×20 mm^2 was used. This is based on assumption that the stress state and magnitude will

remain constant in the welding direction. The increase in gage volume along the welding direction, in these two directions, allows faster measurement with more grain sampling.

2.3.4 Stress-Free Lattice Parameter Measurement. In determining residual stress using neutron diffraction, it is important to correct the measured strain for compositional variation. Therefore, the stress-free comb machined out from the weld is measured for spatial correction of the measured strain in the plate. The comb-shaped sample of dimension 6 mm × 6 mm × 5 mm was machined out from the parent plate by electrical discharge machining. This dimension of the comb would ensure relaxation of any macroresidual stress field. The comb geometry would also allow positional correction of the measured strain for compositional variation across the weld and also any changes in lattice parameter due to intergranular straining (Ref 19, 20). The stress-free lattice spacing (d_0) were measured in all the three principal strain directions.

The lattice spacing d is related to scattering angle θ by Bragg's law as shown in Eq 2.

$$\lambda = 2d_{\mathrm{hkl}} \sin\left(\frac{\theta}{2}\right), \qquad \text{(Eq 2)}$$

where λ is the wavelength

Gaussian fitting routine was used to fit the intensity profile and precise determination of the peak position. The stress-free lattice spacing (d_0) measurement combined with the lattice spacing measurements was used to calculate strain (ε) along the three principal strain direction using Eq 3.

$$\varepsilon_{\mathrm{hkl}} = \left(\frac{d_{\mathrm{hkl}}}{d_{0\mathrm{hkl}}} - 1\right), \qquad \text{(Eq 3)}$$

where ε is strain in the {hkl} family of crystallographic planes, d is the lattice spacing, d_0 is the strain-free spacing (measured in the same plane).

Once the strain in the principal direction are determined, the principal stresses are then analyzed using the Hooke's law for three-dimensional state of stress as shown in Eq 4, using the appropriate elastic constants for the specific crystallographic plane.

$$\sigma_{ii} = \frac{E}{(1+\upsilon)}\left[\varepsilon_{ii} + \frac{\upsilon}{(1-2\upsilon)}(\varepsilon_{11}+\varepsilon_{22}+\varepsilon_{33})\right], \qquad \text{(Eq 4)}$$

where E is the Young's modulus, υ is the Poisson ratio, i = 1, 2, 3 indicate the component of stress and strain relative to chosen to the principal strain directions.

Elastic constants values of E = 225.5 GPa and υ = 0.28 (Ref 5) are used to calculate stress from measured strains.

3. Results and Discussion

3.1 Temperature–Time Plot

Figure 5 shows the thermal cycle when the sample was heated up to 900 °C using a controlled laser power at constant beam diameter of 110 mm. This temperature was selected based on the fact that recrystallization temperature of structural alloy is between one-third and one-half of the absolute melting temperature (1540 °C for steel) (Ref 21).

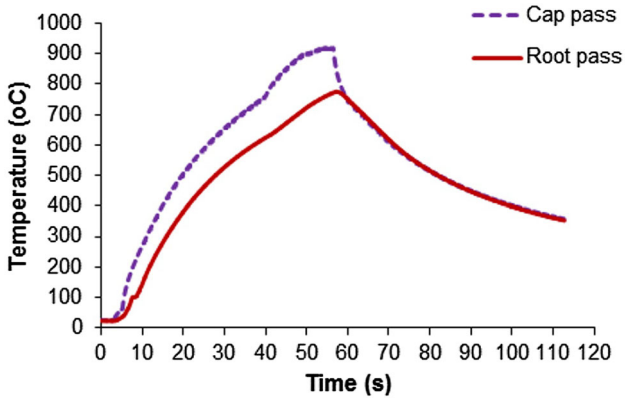

Fig. 5 Thermal cycles of control laser power using a constant beam diameter of 110 mm

3.2 Microstructural Observations

The optical micrographs of both the as-welded and post-weld cold rolled samples were not clearly identified but were believed to consist of martensitic (bainitic) microstructures due to enriched solid solution strengthening element in both the parent metal and the filler wire. For example, silicon (high percentage in the weld metal) is a powerful ferrite strengthener when compared with other alloying elements which promotes considerable hardness through solid solution. This resulted in localized increase in hardenability in the weld and heat-affected region. Previous research conducted by Ibrahim (Ref 22) also confirmed this phenomenon. Post-weld cold rolling resulted in increasing hardening by about 50 HV. Post-weld cold rolling followed by laser processing shows M-A (martensite-austenite) islands present in the microstructure.

EBSD techniques were used for detailed analysis of microstructure. Figure 6 shows the micrographs of all the samples obtained from EBSD. These micrographs were obtained from data collected over an area of 538 μm × 401 μm with step size 0.437 μm. The as-welded and post-weld cold rolled samples have dendritic grains structure with low angle grain boundary (Fig. 6a and b). The post-weld cold rolling followed by laser processing (Fig. 6c) shows clear grains, different grain orientations with high angle grain boundaries. The refined grains obtained by post-weld cold rolling followed by laser processing is known to increase the strength and toughness of the material which is lower in as-welded state due to the formation of dendritic grain structure. These refined grains are also resistant to fatigue and fracture failures.

3.3 Hardness

A hardness scan was performed across the weld metal (cap pass). Hardness values are lowest in the parent metal, but sharply increase in the HAZ, and remain fairly uniform in the weld metal (Fig. 7a). This high hardness at the HAZ is caused by the presence of martensite in the microstructure. The presence of martensite was as a result of the high cooling rate experienced at the zone along with high hardenability due to increased grain size in the HAZ and the alloying elements in the weld metal.

Post-weld cold rolling increases the hardness value from 341 to 400 HV at the weld metal. This effect of post-weld cold rolling could be attributed to work hardening which is inevitable consequence of the plastic deformation induced

during rolling. Post-weld cold rolling followed by laser processing resulted in softening of the weld metal throughout the entire thickness (Fig. 7b). The hardness values drop from 400 to 278 HV at the cap pass (Fig. 7a). This resulted in nucleation of strain-free grains from the cold-worked metal matrix at points of high lattice strain energy. As a consequence, the hardness also decreases. Further cold rolling after post-weld cold rolling followed by laser processing reinstate the hardness profile to as-welded state (278 to 310 HV at the cap pass), indicating the effect of work hardening after laser processing. This cold working leads to plastic deformation of the weld metal and thereby redistribute the residual stress. As observed in Fig. 7(a), increase in hardness in cold rolling after post-weld cold rolling followed by laser processing is less than hardness in post-weld cold rolled condition, because the matrices were tough and have high plasticity.

The hardness scan along the weld metal (Fig. 7b) shows an increase in hardness value of the as-welded sample from the cap to the root pass of the weld metal, indicating that the root pass is harder than the cap pass. The higher hardness in the root pass is a result of thermal straining due to successive deposition of filler wire. The effect of cold working was observed throughout the entire thickness (first cold rolling). However, up to about 4 mm, the effect is more pronounced; after that, from 4 to 10 mm the effect is less pronounced. However, between 10 and 12 mm the hardness is slightly higher than the middle part of the weld which could be attributed to reaction from the backing bar.

3.4 Residual Stress

The residual stress analyzed from the measurements of elastic strain showed a reduction in magnitude from cap to root in as-welded and post-weld cold rolled followed by laser processing. As shown in Fig. 8, the peak tensile residual stress of the as-welded sample diminishes in magnitude through the thickness of a multi-pass weld. The reduction in magnitude is attributed to the fact that multiple passes result in thermal straining of previously laid pass from successive passes. The thermal cycling would cause macroscopic plastic deformation of previously laid passes. However, reduction in peak tensile residual stress of post-weld cold rolled followed by laser processing sample can be attributed to high thermal conductivity and low coefficient of thermal expansion of the ferritic steel as compared to austenitic steel.

The effect of post-weld cold rolling in as-welded condition and further cold rolling after laser processing showed a reduction in peak compressive residual stress through the thickness of a multi-pass weld. This could be attributed to direct contact between local mechanical tensioning (roller) and cap pass indicating the effect of cold working which lead to hardening of the weld metal and thereby redistributing the residual stress.

3.4.1 Effect of Post-Weld Cold Rolling Through the Thickness. Figure 8 shows that the effect of post-weld cold rolling (measurement was taken at 2.5 mm below the top surface) has modified the longitudinal residual stress state causing it to become compressive around the weld metal (from peak tensile stress of 530 MPa to compressive stress of 258 MPa). Application of rolling to the welded joints causes yielding of material in the weld region. This effect compresses the material in the direction normal to the weld's surface leading to hardening of the weld metal and thereby relax the residual stress. The compressive residual stress generation at this region is beneficial in improving the structural integrity of a component as most of the in-service deterioration starts with a surface flaw.

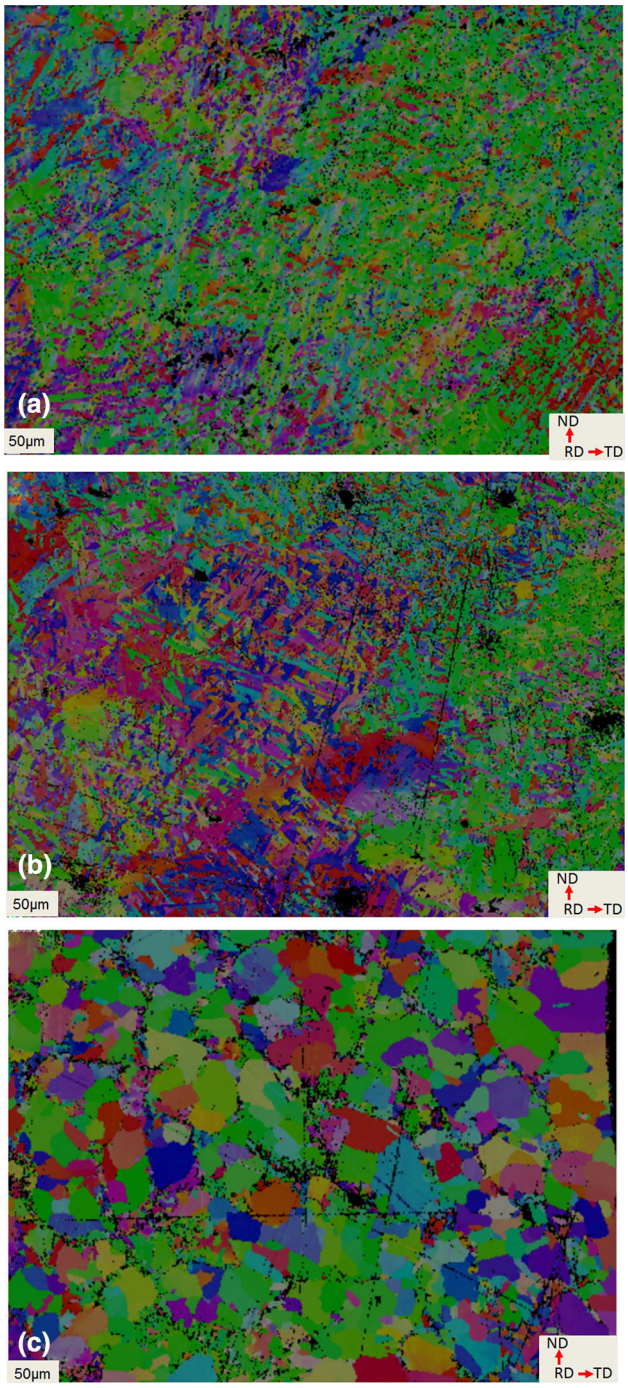

Fig. 6 Showing EBSD micrograph, (a) As-welded (b) Post-weld cold rolled (c) Post-weld cold rolled followed by laser processing

It was observed that, at about 6.5 mm below the top surface (Fig. 8), the rolling load has shown influence on the residual stress state of the weld. The rolling modified the peak tensile stress from 487 MPa to compressive stress of 183 MPa suggesting significant effect of the rolling load at the region. However, at 10.5 mm below the top surface (Fig. 8), the impact of rolling is less pronounced (when compared with 2.5 mm below the weld surface) but still manages to change the tensile as-welded stress to a compressive value in the weld metal.

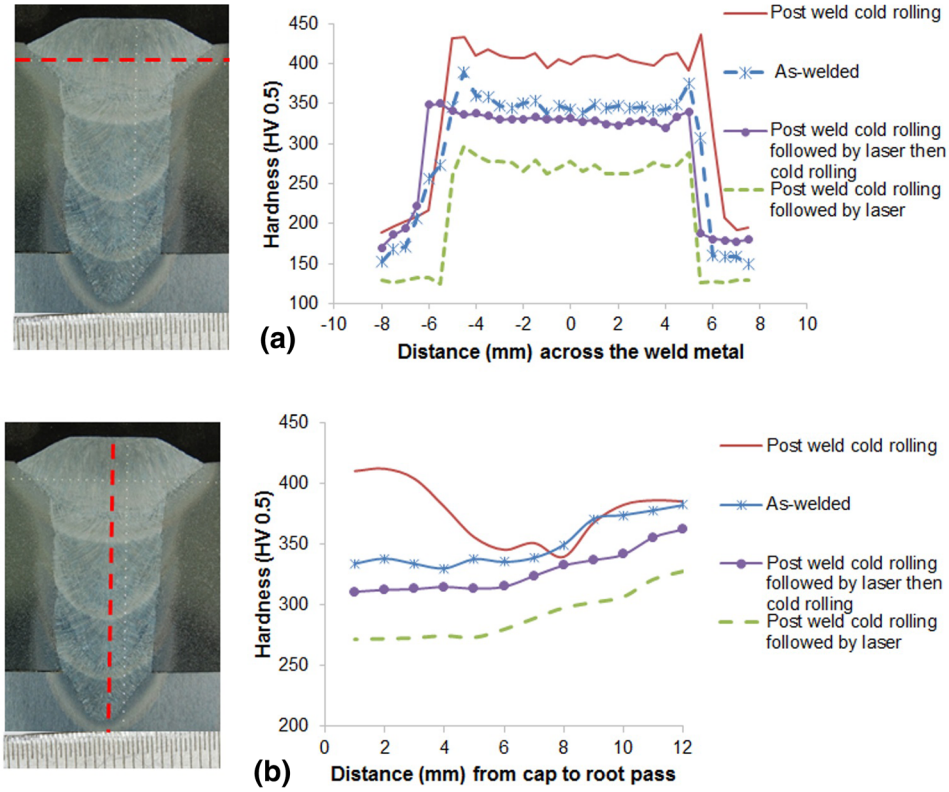

Fig. 7 Showing the hardness profile (a) across the weld metal (b) along the weld metal

3.4.2 Effect of Post-Weld Cold Rolling Followed by Laser Processing. Post-weld cold rolling followed by laser processing (measurement was taken at 2.5 mm below the top surface) has reversed the longitudinal residual stress from compressive stress of 258 MPa to tensile stress of 699 MPa (Fig. 8) indicating a high thermal input and non-uniform cooling of the plate resulting in development of the residual stress in the longitudinal direction. The applied heat generated inhomogeneous plastic deformation and tensile residual stresses.

At about 6.5 mm below the top surface (Fig. 8), application of laser processing to the rolled samples modified the residual stress from compressive stress of 183 MPa to tensile stress of 462 MPa showing a significant effect of heat at the region. Similarly, the effect of the applied thermal energy was pronounced at 10.5 mm below the top surface, indicating that the heat was conducted throughout the entire thickness of the material which causes changes in the residual stress state.

3.4.3 Effect of Cold Rolling After Post-Weld Cold Rolling Followed by Laser Processing. Further cold rolling after laser processing has redistributed and eliminated the tensile residual stress state formed during laser processing throughout the entire thickness of the material. Cold rolling following the laser processing was found to be effective in creating a compressive stress field as expected.

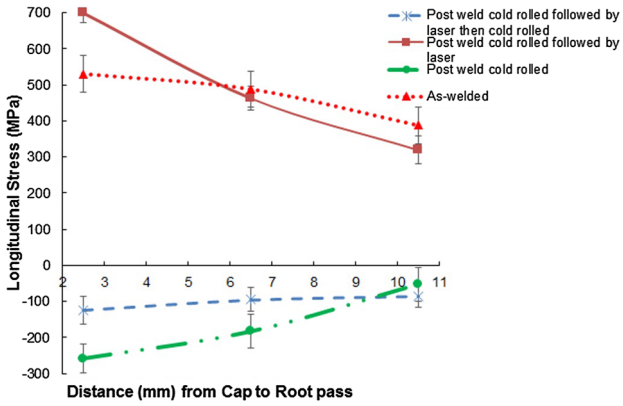

Fig. 8 Residual stress profile variation across the weld in sample with different processing conditions through the thickness

4. Conclusion

Local mechanical tensioning (rolling) followed by laser processing to create a refined and recrystallized microstructure with modified residual stress state, thus improving the fatigue life of welded structures, was investigated. It can be concluded from this research as follows:

1. The effect of rolling was realized throughout the entire thickness of the multi-pass welds that modified the longitudinal residual stress state causing it to become compressive around the weld metal.
2. Grain refinement was observed at the cap pass when post-weld cold rolling followed by laser processing was applied to the sample.

3. Due to thermal straining from successive pass, the tensile residual stress of the as-welded sample diminishes in magnitude through the thickness of a multi-pass weld.
4. Post-weld cold rolling followed by laser processing reinstated as-welded residual stress state profile throughout the entire thickness of the multi-pass welds.
5. Further cold rolling after laser processing has redistributed and eliminated the tensile residual stress state formed during laser processing. Generation of this compressive stress state is beneficial in improving the structural integrity of a component as most of the in-service deterioration starts with a surface flaw.
6. In summary, this novel processing clearly demonstrates the improvement of structural features that can be obtained in traditional welded structural alloys. However, optimisation of the post-weld cold rolling and laser processing would be required for different alloy systems. It would be advisable to consider the material's work hardening characteristics, and the effects of deformation on metallurgical and constitutive properties, if post-weld cold rolling is to be applied.

Acknowledgments

The authors are grateful for the funding provided by Petroleum Development Trust Fund in Nigeria, under the PTDF scholarship scheme no. PTDF/E/OSS/PHD/SJ/391/11. The authors are also thankful to Mr Brian Brooks and Mr Flemming Nielsen for technical support in laboratory. Dr Supriyo Ganguly acknowledges support from EPSRC through grant numbers EP/J017086/1 and EP/K030884/1.

Open Access

Reference

1. R.H. Leggatt, Residual Stresses in Welded Structures, *Int. J. Press. Vessel. Pip.*, 2008, **85**(3), p 144–151
2. J. Mullins and J. Gunnars (2011) *Deformation Histories Relevant to Multipass Girth Welds: Temperature, Stress and Plastic Strain Histories*, Riva del Garda, Trento ed
3. J.A. Francis, H.K.D.H. Bhadeshia, and P.J. Withers, Welding Residual Stresses in Ferritic Power Plant Steels, *Mater. Sci. Technol.*, 2007, **23**(9), p 1009–1020
4. S. Kou, *Welding Metellury*, 2nd ed., Wiley, Hoboken, 2003
5. H.E. Coules, L.D. Cozzolino, P. Colegrove, S. Ganguly, S.W. Wen, and T. Pirling, Neutron Diffraction Analysis of Complete Residual Stress Tensors in Conventional and Rolled Gas Metal Arc Welds, *Exp. Mech.*, 2012, **53**(2), p 195–204
6. D.J. Smith and S.J. Garwood, Influence of Postweld Heat Treatment on the Variation of Residual Stresses in 50 mm Thick Welded Ferritic Steel Plates, *Int. J. Press. Vessel. Pip.*, 1992, **51**(2), p 241–256
7. J.S. Porowski, W.J. O'Donnell, M.L. Badlani, and E.J. Hampton, Use of the Mechanical Stress Improvement Process to Mitigate Stress Corrosion Cracking in BWR Piping Systems, *Nucl. Eng. Des.*, 1990, **124**(1–2), p 91–100
8. D.G. Richards, P.B. Prangnell, S.W. Williams, and P.J. Withers, Global Mechanical Tensioning for the Management of Residual Stresses in Welds, *Mater. Sci. Eng. A*, 2008, **489**(1–2), p 351–362
9. S.A. Kurkin and V.I. Anufriev, Preventing Distortion of Welded Thin-Walled Members of AMg6 1201 Aluminium Alloys by Rolling the Weld with a Roller Behind the Welding Arc, *Weld. Prod. (English translation of Svarochnoe Proizvodstvo)*, 1984, **31**(10), p 52–55
10. S.A. Kurkin, V.I. Anufriev, and E.S. Milekhin, Improving the Mechanical Properties of Welded Joints in the AMg6 Alloy by Plastic Deformation During Arc Welding, Svarochnoe Proizvodstvo, *Weld. Prod.*, 1980, **27**, p 20–24
11. W. Liu, X. Tian, and X. Zhang, Preventing Weld Hot Cracking by Synchronous Rolling During Welding, *Weld. J. (Miami, Fla)*, 1996, **75**(9), p 297
12. H.E. Coules, P. Colegrove, L.D. Cozzolino, S.W. Wen, S. Ganguly, and T. Pirling, Effect of High Pressure Rolling on Weld-Induced Residual Stresses, *Sci. Technol. Weld. Join.*, 2012, **17**(5), p 394–401
13. J. Altenkirch, A. Steuwer, P.J. Withers, S.W. Williams, M. Poad, and S.W. Wen, Residual Stress Engineering in Friction Stir Welds by Roller Tensioning, *Sci. Technol. Weld. Join.*, 2009, **14**(2), p 185–192
14. S. Jibrin, G. Supriyo, C. Harry, and P. Thilo, Comparative Study of Evolution of Residual Stress State by Local Mechanical Tensioning and Laser Processing of Ferritic and Austenitic Structural Steel Welds, *J. Mech. Eng. Autom.*, 2015, **5**(1), p 33–42
15. M.T. Hutchings, *Introduction to the Characterization of Residual Stress by Neutron Diffraction*, CRC Press, Boca Raton, 2005
16. T. Pirling, G. Bruno, and P.J. Withers, SALSA-A New Instrument for Strain Imaging in Engineering Materials and Components, *Mater. Sci. Eng. A*, 2006, **437**(1), p 139–144
17. P.J. Withers, M. Turski, L. Edwards, P.J. Bouchard, and D.J. Buttle, Recent Advances in Residual Stress Measurement, *Int. J. Press. Vessel. Pip.*, 2008, **85**(3), p 118–127
18. X. Wang, S. Spooner, and C.R. Hubbard, Theory of the Peak Shift Anomaly due to Partial Burial of the Sampling Volume in Neutron Diffraction Residual Stress Measurements, *J. Appl. Crystallogr.*, 1998, **31**(1), p 52–59
19. M. Rogante, Stress-Free Reference Sample: The Problem of the Determination of the Interplanar Distance d0, *Physica B: Condens. Matter*, 2000, **276–278**, p 202–203
20. T.M. Holden, H. Suzuki, and D.G. Carr, Macroscopic Stress Measurements by Neutron Diffraction and the Part Played by the "Stress-Free" Reference, *ISIJ Int.*, 2006, **46**(7), p 959–965
21. D.C. William (2007) *Material Science & Engineering: An Introduction,* 7th ed., USA
22. N.K. Ibrahim (2011) "Effect of Welding Thermal Cycle on the Heat Affected Zone Microstructure and Toughness of Multi-pass Welded Pipeline Steels", (PhD Thesis), Cranfield University, Cranfield, UK,